Polymer 121 (2017) 9–16

Contents lists available at ScienceDirect

Polymer

journal homepage: www.elsevier.com/locate/polymer

Synthesis and gas permeation properties of a novel thermally-rearranged polybenzoxazole made from an intrinsically microporous hydroxyl-functionalized triptycene-based polyimide precursor

Fahd Alghunaimi, Bader Ghanem, Yingge Wang, Octavio Salinas, Nasser Alaslai, Ingo Pinnau*

King Abdullah University of Science and Technology, Advanced Membranes and Porous Materials Center, Division of Physical Sciences and Engineering, Program of Chemical and Biological Engineering, Thuwal 23955-6900, Saudi Arabia

ARTICLE INFO

Article history:
Received 17 February 2017
Received in revised form
2 May 2017
Accepted 4 June 2017
Available online 6 June 2017

Keywords:
Gas separations
Polyimide
Triptycene
Thermal rearrangement
Polybenzoxazole

ABSTRACT

A hydroxyl-functionalized triptycene-based polyimide of intrinsic microporosity (TDA1-APAF) was converted to a polybenzoxazole (PBO) by heat treatment at 460 °C under nitrogen atmosphere. TDA1-APAF treated for 15 min (TR 460) resulted in a PBO conversion of 95% based on a theoretical weight loss of 11.7 wt% of the polyimide precursor. The BET surface area of the TR 460 (680 m^2 g^{-1}) was significantly higher than that of the TDA1-APAF polyimide (260 m^2 g^{-1}) as determined by nitrogen adsorption at −196 °C. Heating TDA1-APAF for 30 min (TRC 460) resulted in a weight loss of 13.5 wt%, indicating full conversion to PBO and partial main-chain degradation. The TR 460 membrane displayed excellent O_2 permeability of 311 Barrer coupled with an O_2/N_2 selectivity of 5.4 and CO_2 permeability of 1328 Barrer with a CO_2/CH_4 selectivity of 27. Interestingly, physical aging over 150 days resulted in enhanced O_2/N_2 selectivity of 6.3 with an O_2 permeability of 185 Barrer. The novel triptycene-based TR 460 PBO outperformed all previously reported APAF-polyimide-based PBOs with gas permeation performance close to recently reported polymers located on the 2015 O_2/N_2 upper bound. Based on this study, thermally-rearranged membranes from hydroxyl-functionalized triptycene-based polyimides are promising candidate membrane materials for air separation, specifically in applications where space and weight of membrane systems are of utmost importance such as nitrogen production for inert atmospheres in fuel lines and tanks on aircrafts and off-shore oil- or natural gas platforms. Mixed-gas permeation experiments also demonstrated good performance of the TR 460 membrane for natural gas sweetening with a CO_2 permeability of ~1000 Barrer and CO_2/CH_4 selectivity of 22 at a typical CO_2 wellhead partial pressure of 10 bar.

1. Introduction

Membrane-based gas separation is a well-established industrial technology with great potential for a wide diversity of large-scale industrial applications, such as natural gas sweetening, hydrogen recovery, CO_2 separation from flue gas, and air separation [1–3]. It was estimated in 2002 that ~50% of the membrane-based gas separation market was based on onsite nitrogen production from air [3]. The success of membranes in air separation can be attributed to the ubiquitous clean feed gas, a simple single-stage process design and the delivery of the nitrogen product gas at feed pressure. Commercial polymeric membrane materials, including tetrabromopolycarbonate, Matrimid® polyimide and polysulfone, are offering selectivities of ~6–7 that can produce 99% nitrogen but with low oxygen permeability of ~1–2 Barrer [3]. Currently, poly(phenylene oxide) is the most permeable polymer membrane used for *commercial* air separation with an oxygen permeability of 16 Barrer and O_2/N_2 selectivity of 4.9 [4]. It is interesting to note that these commercial air separation membrane materials fall far below the O_2/N_2 permeability/selectivity trade-off curve reported by Robeson in 1991 [5]. Hence, there is a strong incentive for development of advanced polymers that exhibit better performance for air

* Corresponding author. King Abdullah University of Science and Technology, Advanced Membranes and Porous Materials Center, Division of Physical Sciences and Engineering, Chemical and Biological Engineering Program, Al-Jazri Bldg. 4, Thuwal 23955-6900, Saudi Arabia.
E-mail address: ingo.pinnau@kaust.edu.sa (I. Pinnau).

http://dx.doi.org/10.1016/j.polymer.2017.06.006
0032-3861/

separation. Specifically, in applications where space and membrane system weight limitations play a major role, such as nitrogen blanketing of fuel tanks on aircrafts and oil and natural gas offshore platforms, require polymer membranes with higher permeability without significant loss of O_2/N_2 selectivity compared to commercial air separation membranes.

Polymers of intrinsic microporosity (PIMs), first introduced by Budd and McKeown in 2004, are a rapidly expanding class of amorphous glassy ladder polymers [6,7]. PIMs have an inherent, interconnected porosity with micropores of less than 20 Å resulting from inefficient packing of polymer chains in the solid state [8,9]. PIM-1 (Fig. 1), the prototype of this materials class is a spirobisindane-based ladder polymer, which has a Brunauer-Teller-Emmett (BET) surface of ~860 m g^{-1}, excellent solution processability and thus good thin-film formation properties. Furthermore, PIM-1 and a related bis(phenazyl)-derived spirobisindane ladder polymer (PIM-7) demonstrated very high gas permeability and moderate selectivity for a variety of gas pairs, defining the 2008 upper bound for O_2/N_2 separation [10].

More recently, intrinsically microporous polyimides (PIM-PIs) were developed with performance close to the 2008 upper bounds for several important gas pairs [11–14]. Ghanem et al. [11,12] and Rogan et al. [15] reported the first series of PIM-PIs based on spirobisindane dianhydrides and various diamines, which displayed excellent gas permeability with moderate selectivity. Thereafter, PIM-PIs with enhanced selectivity were prepared with newly designed sterically hindered monomers based on spirobifluorene-, ethanoanthracene-, Tröger's base-, and triptycene-building blocks [12–20]. Recently, our group synthesized TDA1-APAF, a hydroxyl-functionalized triptycene-based PIM-PI (Fig. 1), which exhibited notable performance for O_2/N_2 and CO_2/CH_4 separation [21].

An alternative method to introduce microporosity into glassy polymers is based on the formation of polybenzoxazoles (PBO) by a high-temperature (>400 °C) decarboxylation and rearrangement reaction of polyimide precursors bearing hydroxyl-functional groups in ortho-position to the imide linkages [22]. In 2007, Park et al. reported gas permeation properties of a family of thermally-rearranged (TR) PBO polymers, which exhibited: (i) exceptional CO_2 permeability and good CO_2/CH_4 selectivity, (ii) resistance to plasticization, and (iii) excellent chemical stability [22–24]. Using soluble hydroxyl-functionalized polyimide precursors allows fabrication of hollow fibers using conventional technology and subsequent conversion of the polyimides to PBOs by thermal treatment with desirable transport properties [25,26]. Most TR-derived PBO polymers are based on low-free-volume polyimide precursors made from 4,4'-(hexafluoroisopropylidene)diphthalic anhydride (6-FDA) and 2,2′-bis(3-amino-4-hydroxyphenyl)-hexafluoropropane (APAF) or 3,3'-dihydroxy-4,4'-diamino-biphenyl (HAB) [23,24,27–32]. So far, only a few reports described the use of hydroxyl-functionalized intrinsically microporous polyimides (PIM-PIs) as precursors for the formation of PBOs, including spirobisindane- and spirobifluorene-based building blocks [33–36]. Recently, a PBO derived from a low-free-volume triptycene dianhydride/APAF-based polyimide (TPHI) showed commendable gas separation performance. The PBO made by heat treatment of TPHI at 400 °C for 2 h (PBO conversion of 87% based on theoretical weight loss of 9.7 wt% for full conversion) showed CO_2, N_2, and CH_4 permeabilities of 320, 16 and 8.3 Barrer, respectively, combined with CO_2/N_2 and CO_2/CH_4 selectivities of 20 and 39 [32]. Unfortunately, O_2 permeability data were not reported in this work.

Here, we report the synthesis (Scheme 1) and gas transport properties of a TR membrane prepared from a recently reported intrinsically microporous triptycene-based hydroxyl-functionalized PIM-PI [21]. The pristine polyimide was prepared by a one-step polycondensation reaction between a commercial hydroxyl-containing diamine monomer (APAF) and 9,10-dimethyl-2,3,6,7-triptycene tetracarboxylic dianhydride (TDA1) monomer, as previously reported by our group [21,37]. The TR membranes were characterized by FTIR, BET, XRD and TGA measurements. Additionally, pure-and mixed-gas permeation properties of pristine TDA1-APAF and TDA1-APAF-derived TR membranes (fresh and physically aged) were performed to demonstrate their potential as highly permeable and selective membranes for air and natural gas separation applications.

2. Experimental

2.1. Materials

The compounds 1,2-dimethoxybenzene, 2-aminobenzoic acid, trifluoromethanesulfonic anhydride, acetic anhydride, 1,1′-bis(diphenylphosphino)ferrocene, tris(dibenzylideneacetone) dipalladium(0), boron tribromide (BBr_3), zinc cyanide, potassium hydroxide, and isoquinoline were obtained from Aldrich and used as received. 9,10-Dimethyl-2,3,6,7-triptycene tetracarboxylic dianhydride (TDA1) monomer was synthesized as previously described [37]. The monomer 2,2′-bis(3-amino-4-hydroxyphenyl)-hexafluoropropane (APAF) was purchased from Aldrich and purified by vacuum sublimation at 220 °C. *m*-Cresol was distilled under reduced pressure and stored under nitrogen in the dark over 4 Å molecular sieves. All other solvents were obtained from various commercial sources and used as received [21].

2.2. Polymer characterization of pristine and thermally rearranged TDA1-APAF membranes

Fourier transform infrared (FTIR) measurements were carried out using a Varian 670-IR spectrometer. Thermogravimetric analysis (TGA) was performed with a TG 209 F1 (Netzsch) coupled with a NETZSCH QMS 403 C Aëolos® mass spectrometer (MS) under nitrogen atmosphere with a heating rate of 5 °C/min up to 800 °C. The BET surface areas of the pristine TDA1-APAF and TR 460 were determined by N_2 sorption at −196 °C using a Micromeritics ASAP-2020. Powder samples were degassed under high vacuum at 120 °C

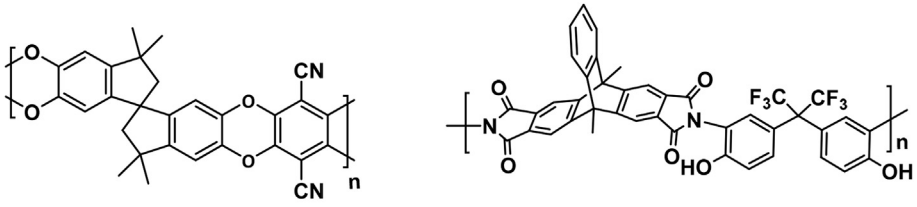

PIM-1 TDA1-APAF

Fig. 1. Structures of PIM-1 and OH-functionalized PIM-PI (TDA1-APAF).

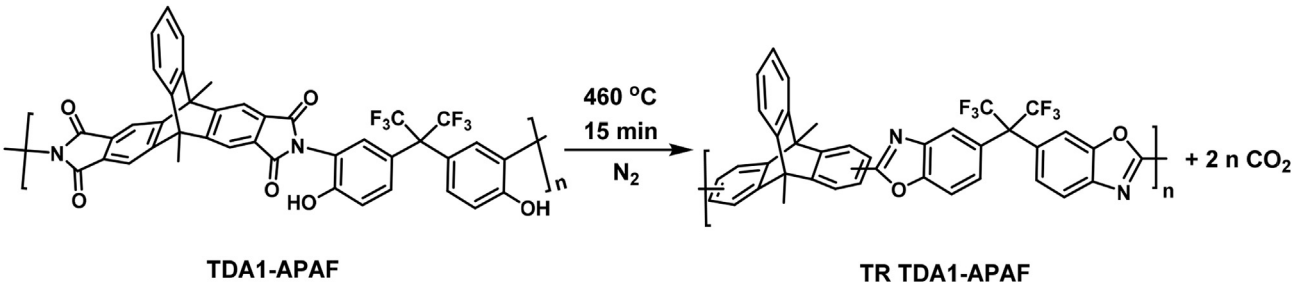

Scheme 1. Synthesis of TDA1-APAF-derived TR membrane.

for 15 h prior to analysis. Analysis of the pore size distributions was performed using the NLDFT (Non-Local Density Functional Theory) model using N_2 (at −196 °C) sorption isotherms for carbon-slit pore geometry provided by ASAP-2020 version 4.02 software. Wide-angle x-ray diffraction (WAXD) patterns of the fresh and aged TR 460 films were recorded in the reflection mode at room temperature on a Bruker D8 Advance diffractometer (wavelength λ = 1.54 Å). The average d-spacing values of the polymers were calculated using Bragg's law in the 2θ range of 7–40°.

2.3. Synthesis of TDA1-APAF, polymer film preparation and thermal conversion

A mixture of TDA1 (0.23 g, 0.54 mmol), APAF (0.2 g, 0.54 mmol) and 3 ml *m*-cresol was stirred in a Schlenk tube for 30 min under nitrogen at room temperature. The mixture was heated at 80 °C for 1 h and 3 drops of isoquinoline were added as catalyst. The temperature was then raised gradually to 200 °C and kept at that temperature until the mixture became very viscous. Water formed during imidization was removed with a stream of nitrogen. After cooling, the polyimide solution was added into methanol (250 ml) and the crude fibrous polymer was filtered, washed with methanol and dried. Re-precipitation by a THF–methanol mixture was carried out twice for further purification and the polymer was finally dried at 120 °C in a vacuum oven for 24 h to give 86% yield as previously reported [21]. A polymer solution (5 wt/vol%) in THF was filtered through 0.45 μm polypropylene filters, poured onto a flat glass Petri dish and slowly evaporated at room temperature for one day. The obtained membrane was dried at 120 °C. To remove any traces of residual solvent, the membrane was soaked in methanol for 10 h, air-dried, and then post-dried at 250 °C in a vacuum oven for 12 h.

Polyimide (TDA1-APAF) film samples were converted to PBOs membranes by thermal treatment in a Carbolite tubular furnace. Pyrolysis was conducted under nitrogen flow and polymer samples were sandwiched between two ceramic plates. Metal spacers were inserted between the ceramic plates to allow nitrogen to continuously flush the samples. The oxygen concentration in the furnace was monitored with an O_2 analyser (Cambridge Sensotech, Rapidox 3100). Ramping of the treatment temperature did not begin until the O_2 concentration was less than 2 ppm. The thermally rearranged membranes were made at a rate of 10 °C/min from room temperature to 460 °C where it was held isothermally for 15 and 30 min to achieve conversion of the polyimide to PBO. The furnace was then shut off and the film was left to cool to room temperature under continuous nitrogen flow. Film thickness and effective area for gas permeation measurements were determined by a digital micrometer and scanner, respectively. PBO films with thickness of 70 ± 5 μm were used for gas permeation experiments. Samples for long-term physical aging studies were stored in a desiccator under vacuum.

2.4. Pure-gas permeation experiments

The pure-gas permeabilities of thermally rearranged (TR) TDA1-APAF membranes were determined by using the variable pressure/constant volume method. The polymer film sample was degassed in the permeation cell under vacuum for at least 24 h. The pure-gas permeability of He, H_2, N_2, O_2, CH_4, and CO_2 was measured at 35 °C and 2 bar. The gas permeability was calculated by:

$$P = 10^{10}\frac{V_d l}{P_{up} A R T}\frac{dp}{dt}$$

where P is the permeability in Barrers (1 Barrer = 10^{-10} cm^3(STP) cm/cm^2 s cmHg), p_{up} is the upstream pressure (cmHg), dp/dt is the steady-state permeate-side pressure increase (cmHg/s), V_d is the calibrated permeate volume (cm^3), l is the membrane thickness (cm), A is the effective membrane area (cm^2), T is the operating temperature (K), and R is the gas constant (0.278 cm^3 cmHg/cm^3(STP) K). The ideal pure-gas selectivity for a gas pair is given by the following relationship:

$$\alpha_{A/B} = \frac{P_A}{P_B}$$

The apparent diffusion coefficient D (cm^2/s) was calculated by $D = l^2/6\theta$, where θ is the time lag of the permeability measurement and l is the membrane thickness. The solubility coefficient S (cm^3(STP)/cm^3 cmHg) was then calculated from the solution-diffusion gas transport relationship: S = P/D.

2.5. Mixed-gas permeation experiments

The mixed-gas permeation measurements of TR 460 were performed at 35 °C using a custom-designed mixed-gas permeation system similar to that described by O'Brien et al. [39]. The feed gas mixture contained 50 vol% CH_4/50 vol% CO_2 and the total feed pressure was varied between 4 and 30 bar; the permeate pressure was less than 0.01 bar. The permeate flow rate to feed flow rate, i.e. the stage-cut, was set at 0.01. Applying these conditions, the residue composition was essentially equal to that of the feed gas and concentration polarization effects could be neglected. CO_2 and CH_4 permeate concentrations were detected with a gas chromatograph (Agilent 3000 A Micro GC) equipped with a thermal conductivity detector. The CO_2/CH_4 mixed-gas permeability was calculated by:

$$P_{CO_2} = 10^{10}\frac{y_{CO_2} V_d L}{x_{CO_2} p_{up} A R T}\frac{dp}{dt}$$

$$P_{CH_4} = 10^{10}\frac{y_{CH_4} V_d L}{x_{CH_4} p_{up} A R T}\frac{dp}{dt}$$

where y and x are the mole fractions in the permeate and feed, respectively.

The mixed-gas CO_2/CH_4 selectivity was obtained from:

$$\alpha_{CO_2} = \frac{y_{CO_2}/y_{CH_4}}{x_{CO_2}/x_{CH_4}}$$

3. Results and discussion

3.1. Thermal rearrangement of TDA1-APAF polyimide to polybenzoxazole

The thermal behavior of TDA1-APAF was investigated by TGA-MS to set up optimum thermal conditions for conversion of the polyimide to the corresponding TR-derived PBO. As shown in Fig. 2, a suitable TR range was identified approximately between 400 and 500 °C. It is interesting to note the TGA weight loss curve of the TDA1-APAF did not show the typical two-step decomposition profile commonly observed for hydroxyl-functionalized polyimides, where the first step occurs due to evolution of CO_2 during the formation of PBO and the second step results from main-chain degradation. The evolution of CO_2 during the heating cycle was clearly identified by mass spectroscopy and followed the general trend of the weight-loss derivative curve (Fig. 2).

Additional TGA experiments were performed on three samples with different holding temperatures of 400, 430 and 460 °C, respectively. Initially, the PIM-PI film samples were heated at a rate of 5 °C/min and then kept isothermally for 1 h at each temperature while continuously tracing the weight reduction, as shown in Fig. 3. The weight loss of samples made at 400, 430 and 460 °C for 1 h were 3.0, 5.0 and 13.3 wt% respectively. Based on these results it appeared that the heat treatments at 400 and 430 °C over a duration of 1 h were insufficient to obtain high conversion of the TDA1-APAF to the PBO. Alternatively, a 1-h treatment at 460 °C resulted in

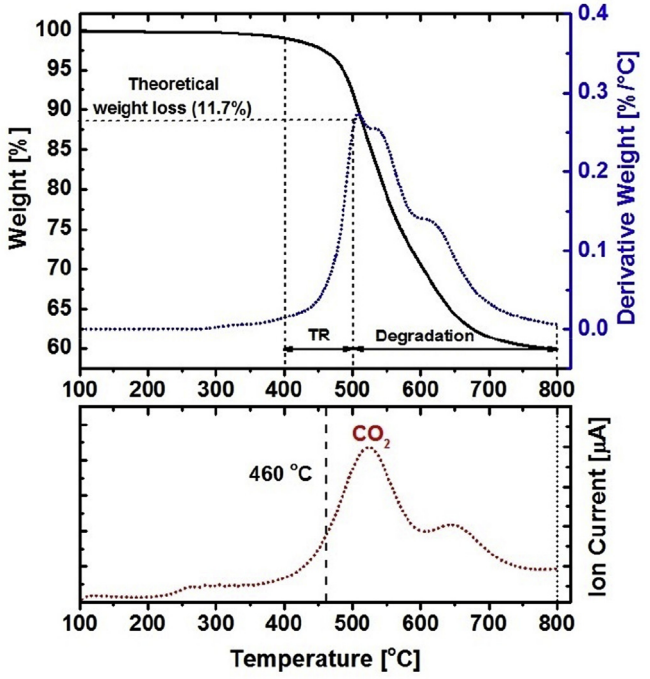

Fig. 2. TGA/MS analysis of TDA1-APAF polyimide film.

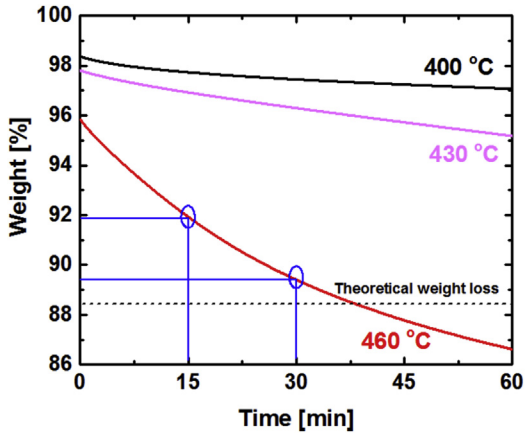

Fig. 3. Time-dependent TGA analysis of TDA1-APAF polyimide films held at isothermal temperatures of 400, 430 and 460 °C, respectively.

formation of a partially degraded PBO membrane as indicated by the higher degree of conversion (13.3 wt%) compared to the theoretical maximum PBO conversion value of 11.7 wt%. Therefore, heat treatment at 460 °C with shorter holding times of 15 (~69% conversion) and 30 min (~91% conversion), respectively, was chosen for formation of TDA1-APAF-derived TR membranes.

TR conversion, as presented in Table 1, is defined as the ratio of the *actual* mass loss after cooling from the treatment temperature to ambient temperature upon thermal rearrangement to the theoretical mass loss [25]:

This calculation was based on the assumption that any polyimide segment that underwent thermal rearrangement was converted to its corresponding PBO segment. The implications and limitations of this methodology have been discussed by Sanders et al. [38]. The total weight loss of the two TDA1-APAF membrane samples after thermal treatment in the Carbolite tubular furnace at 460 °C for 15 and 30 min, and subsequent cooling to room temperature, was 11.1 and 13.5 wt%, respectively. Clearly, the 15-min treatment with cooling cycle to room temperature gave the optimum TR conversion of 95% (referred to as TR 460), whereas the 30-min treatment resulted in some *main-chain degradation* as indicated by an additional weight loss of 1.8% relative to the theoretical value of 11.7 wt% for 100% PBO conversion (referred to as TRC 460). Full characterization of the TRC 460 membrane was outside the main scope of this work; therefore, only pure-gas permeation data are provided below to show the effect of partial carbonization on the gas transport properties of the PBO membranes.

3.2. Characterization of pristine TDA1-APAF and TR 460 membranes

Our previous study on the pristine TDA1-APAF polyimide synthesized from 9,10-dimethyl-2,3,6,7-triptycene tetracarboxylic dianhydride (TDA1) [37] and a commercially available 2,2-bis(3-amino-4-hydroxyphenyl)-hexafluoropropane (APAF) diamine monomer offered a PIM-PI with moderately high BET surface area of 260 m^2/g. The TDA1-APAF membrane had O_2 and CO_2 permeabilities of 8.5 and 40 Barrer coupled with O_2/N_2 and CO_2/CH_4 selectivities of 5.7 and 55, respectively. In this study, TDA1-APAF was used as precursor polymer for the formation of a PIM-triptycene-based PBO. The FTIR spectra for the pristine TDA1-APAF and TR 460, shown in Fig. 4, confirmed the conversion of the polyimide to the PBO as the TR 460 film showed essentially no peaks around 3400 cm^{-1}, which indicated the absence of hydroxyl groups after thermal treatment. Moreover, the TDA1-APAF precursor polymer had characteristic imide peaks at approximately 1779 and

Table 1
Thermal rearrangement conditions and TR conversions for TDA1-APAF film samples in this study.

Sample	Rearrangement temperature (°C)	Time at rearrangement temperature (min)	TR conversion (%)
TR 460	460	15	95
TRC 460	460	30	>100[a]

[a] Additional weight loss of 1.8% due to main-chain degradation.

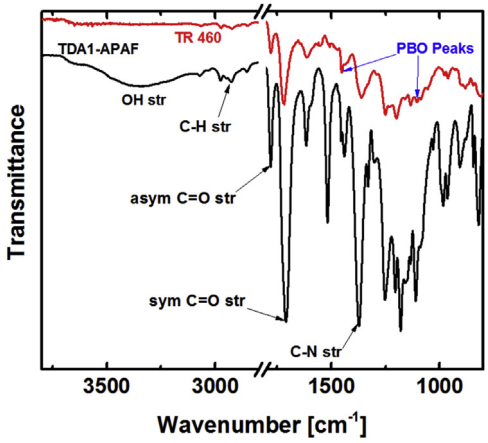

Fig. 4. FTIR spectra for the pristine TDA1-APAF and thermally rearranged TR 460 film.

1710 cm^{-1} which were significantly reduced for the thermally rearranged sample while two characteristic PBO peaks at ~1450 and 1103 cm^{-1} emerged, as noted in previous studies [23,40–42].

The changes in the transformation of the pristine TDA1-APAF polyimide to its TR 460 derivative can be assessed from N_2 (−196 °C) physisorption isotherms (Fig. 5a). The BET surface area of the TDA1-APAF increased significantly from 260 to 680 $m^2\ g^{-1}$ by thermal rearrangement to the TR 460. The corresponding NLDFT-derived pore size distributions (PSDs) are shown in Fig. 5b. The PSDs based on N_2 isotherms showed that the quantity of micropores (>7 Å) increased significantly in TR 460, which correlates qualitatively well with significantly higher gas permeability as compared to the pristine TDA1-APAF, as discussed below. Interestingly, TR 460 also contained a larger fraction of ultramicropores <7 Å compared to TDA1-APAF, which is expected to have a positive effect on gas pair selectivity.

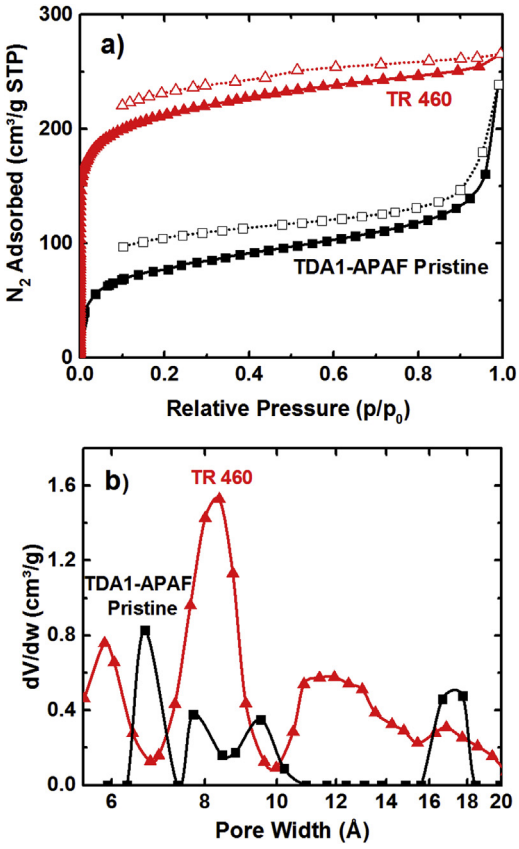

Fig. 5. a) Physisorption isotherms for TDA1-APAF and TR 460 using N_2 at −196 °C. Closed symbols: adsorption; open symbols: desorption. b) NLDFT-based estimated pore size distribution obtained from N_2 isotherms for TDA1-APAF and TR 460 assuming carbon slit-pore geometry.

3.3. Pure-gas permeation properties of fresh and physically aged TR 460 membranes

Pure-gas permeation experiments at 2 bar and 35 °C were performed on two freshly prepared thermally treated film samples of TR 460 (15 min) and TRC 460 (30 min), as shown in Table 2. As expected, the fresh thermally treated samples showed a significant increase in gas permeabilities and a decrease in pure-gas selectivities for all gas pairs relative to the pristine TDA1-APAF polyimide sample. For example, the CO_2 permeability of TDA1-APAF of 40 Barrer increased 33-fold for the 15-min heated TR 460 sample to 1328 Barrer coupled with a large decrease in CO_2/CH_4 selectivity from 55 for the pristine polyimide to 27 for the TR 460 sample. This result was caused by an increase in BET surface area (Fig. 5a) and shift to a significantly larger fraction of pores >7 Å in the TR 460 sample, as indicated by the PSD shown in Fig. 5b. It is noteworthy that the TR 460 membrane showed only a small decrease in O_2/N_2 selectivity to 5.4 from 5.7 for the pristine polyimide, while the O_2 permeability increased 37-fold from 8.5 to 311 Barrer. The partially degraded TRC 460 film exhibited significantly higher gas permeabilities than the pure PBO TR 460 film with only slightly lower gas pair selectivities.

Typically, glassy polymers undergo a physical aging process in which the chains slowly turn into a more tightly packed arrangement towards their equilibrium glassy state [43,44]. Thus, pure-gas permeation experiments were also performed on an aged TR 460 sample after 150 days at 2 bar and 35 °C (Table 2). The permeabilities for all gases decreased for the aged TR 460 membrane; for example, the O_2 permeability decreased from 311 (fresh TR sample) to 185 Barrer (aged TR sample) but O_2/N_2 selectivity increased significantly to 6.3 from 5.4 for the fresh TR sample. Furthermore, the aged TR membrane exhibited an unexpected increase in O_2/N_2 selectivity relative to that of the pristine polyimide precursor.

To shed some light on the differences in chain packing of the fresh and aged TR 460 film samples, wide-angle x-ray diffraction (WAXD) measurements were conducted, as shown in Fig. 6. Both samples showed broad amorphous peaks at low scattering angles 2θ from ~10 to 20°; however, a clear shift of the spectra to higher scattering angles 2θ (lower average d-spacing) was observed for the aged TR 460 sample. In addition, the intensity of the shoulder peak

Table 2
Pure-gas permeabilities and ideal selectivities for pristine TDA1-APAF and thermally rearranged TR 460 and TRC 460 PBOs compared with previously reported APAF-based PBOs.

Polymer	Pure-gas permeability (Barrer)						Ideal selectivity (α)		
	He	H_2	N_2	O_2	CH_4	CO_2	O_2/N_2	H_2/N_2	CO_2/CH_4
TDA1-APAF [21]	92	94	1.5	8.5	0.73	40	5.7	63	55
TR 460[a]	703	1547	58	311	49.4	1328	5.4	27	27
Aged TR 460[b]	(664)	(1304)	(29.4)	(185)	(20.1)	(699)	(6.3)	(44)	(35)
TRC 460[a]	1013	2264	109	511	99.5	2386	4.7	21	24
TR 6FDA-APAF [27]	356	408	19	81	12	398	4.3	22	34
TR 6FDA-APAF [28]	269	294	12.6	52.5	7.5	261	4.2	23	35
TR BPDA-bisAPAF [24]	–	444	20	93	15	597	4.7	22	40
TR PMDA-bisAPAF [30]	–	635	34	148	23	952	4.4	19	41
TR BPDA-bisAPAF [31]	–	1228	48	220	41	1014	4.6	26	25
TPHI-TR-400 [32]	–	520	16	–	8.3	320	–	32	39

[a] This study. Tested after 1 day (at 2 bar; 35 °C).
[b] This study. Tested after 150 days (at 2 bar; 35 °C).

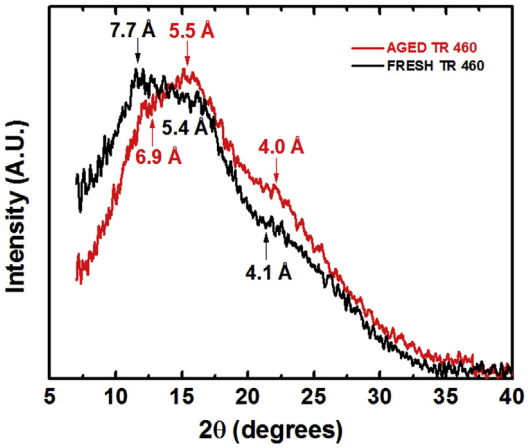

Fig. 6. Wide-angle x-ray diffraction spectra of fresh and aged TR 460 film samples.

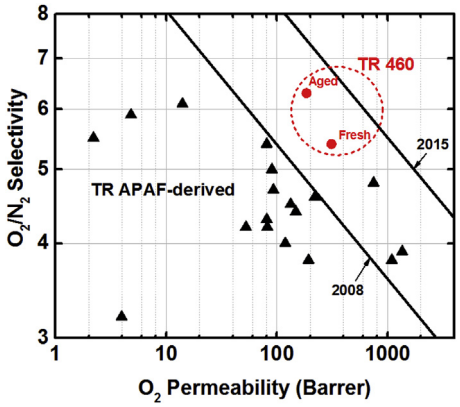

Fig. 7. Pure-gas O_2/N_2 separation performance of previously reported APAF-polyimide-based PBOs [29,30] and TDA1-APAF-derived TR 460 membrane (this study). The solid lines represent 2008 [10] and 2015 [45] permeability/selectivity trade-off curves.

around 22° (d-spacing of ~4 Å) was significantly enhanced in the aged TR 460 sample. Both trends are qualitatively consistent with densification of the aged sample and the corresponding loss in permeability and increase in selectivity compared to the fresh TR 460 sample.

The pure-gas permeation properties of the TR 460 and TRC 460 membranes are also compared to data of previously reported APAF-polyimide-derived PBOs in Table 2. Clearly, the performance of the newly developed triptycene-based TR 460 membrane was superior to other APAF-derived TR membranes for O_2/N_2 separation, as shown in Fig. 7. In fact, its performance exceeded the 2008 upper bound [10] and was close to the more recently reported 2015 O_2/N_2 upper bound [45].

The pure-gas diffusivity (D) values of the pristine TDA1-APAF and TR 460 films for N_2, O_2, CH_4 and CO_2 were calculated by the time-lag method and are presented in Table 3 together with the solubility (S) coefficients. The increased gas permeabilities of the fresh TR 460 sample resulted from significantly enhanced diffusion coefficients compared to the values of the fresh TDA1-APAF polyimide, whereas much smaller increases were observed in their gas solubilities. The reduction in CO_2/CH_4 permselectivity from 55 for the pristine TDA1-APAF polyimide to 27 for the TR 460 (Table 2) occurred due to a decrease in the CO_2/CH_4 diffusion selectivity from 15.8 to 6.9, as shown in Table 4. As expected, the tighter aged TR 460 membrane displayed lower D and S values compared to the fresh sample (Table 3). Concurrently, the aged TR 460 sample yielded enhanced size-sieving properties and, therefore, higher O_2/N_2, $N_2/$

Table 3
Pure-gas diffusion and solubility coefficients of N_2, O_2, CH_4 and CO_2 for pristine and thermally rearranged (fresh and aged) TDA1-APAF membranes.

Polymer	Diffusion coefficient (10^{-8} cm^2/s)				Solubility coefficient (10^{-2} cm^3(STP)/(cm^3 cmHg))			
	N_2	O_2	CH_4	CO_2	N_2	O_2	CH_4	CO_2
TDA1-APAF[a]	0.82	4.5	0.12	1.9	1.8	1.9	6.1	21.1
Fresh TR 460[b]	17.3	88.2	7.21	49.6	3.35	3.53	6.85	26.8
Aged TR 460[c]	(10.15)	(56.7)	(3.94)	(35.7)	(2.9)	(3.26)	(5.1)	(19.5)

[a] Tested after 1 day [21].
[b] This study. TR at 460 °C (15min). Tested after 1 day.
[c] This study. TR at 460 °C (15min). Tested after 150 days.

Table 4
Diffusivity selectivities and solubility selectivities of pristine and thermally rearranged (fresh and aged) TDA1-APAF films (2 bar; 35 °C).

Polymer	Diffusivity selectivity $(\alpha)_D$			Solubility selectivity $(\alpha)_S$		
	O_2/N_2	N_2/CH_4	CO_2/CH_4	O_2/N_2	N_2/CH_4	CO_2/CH_4
TDA1-APAF[a]	5.5	6.83	15.8	1.06	0.30	3.5
Fresh TR TDA1-APAF[b]	5.1	2.40	6.9	1.05	0.49	3.91
Aged TR TDA1-APAF[c]	5.59	2.58	9.1	1.12	0.57	3.82

[a] Tested after 1 day [21].
[b] This study. TR at 460 °C (15min). Tested after 1 day.
[c] This study. TR at 460 °C (15min). Tested after 150 days.

CH_4 and CO_2/CH_4 diffusivity selectivity values than those of the fresh sample (Table 4).

3.4. Mixed-gas permeation properties of thermally rearranged TDA1-APAF (TR 460)

Commonly, high sorption uptake of condensable gases like CO_2 can dilate glassy polymers, induce increased chain mobility, modify the pore structure and, therefore, significantly affect their gas transport properties. The pure- and mixed-gas permeabilities (Figs. 8 and 9) and selectivities (Fig. 10) were measured using a 1:1 CO_2/CH_4 feed mixture with increasing CO_2 partial pressure (2, 5, 7, 10, 12 and 15 bar) for pristine and thermally rearranged TDA1-APAF samples (TR 460). The pure-gas CO_2 permeabilities in both pristine and the TR membrane decreased with increasing CO_2 partial pressure up to 15 bar (Fig. 8), similar to the behavior of previously reported related PIM-PIs [46–49]. This can be rationalized by a decrease in CO_2 solubility coefficient with pressure as is typically observed in glassy polymers due to their dual-mode sorption behavior. In addition, under mixed-gas permeation conditions competitive sorption occurs between CO_2 and CH_4 for available sorption sites, which may reduce the overall sorbed concentration of each gas in the polymer. As a result, the mixed-gas CO_2 permeability was lower than the pure-gas CO_2 permeability value determined at the same partial pressure.

The mixed-gas CH_4 permeability was also lower than the pure-gas value up to a partial pressure of ~10 bar, as shown in Fig. 9. However, the mixed-gas CH_4 permeability was continuously increasing over the entire range pressure and surpassed the pure-gas value possibly due to some plasticization effects. The mixed-gas permselectivites of CO_2/CH_4 at partial CO_2 pressures up to ~8 bar were slightly higher or equal to those determined under pure-gas conditions (Fig. 9) due to a reduction of the mixed-gas CH_4 permeability by co-permeation of CO_2. This mixed-gas permeation "blocking" effect of the less permeable feed gas component by co-permeation of CO_2 was previously observed for some ladder PIMs [50], PIM-PIs [21,46] and PBOs obtained by thermal rearrangement of polyimides [34,51].

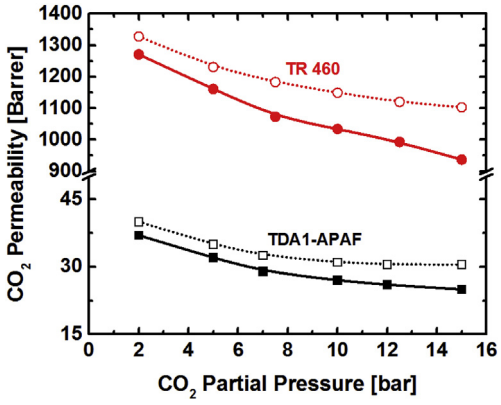

Fig. 8. Pressure-dependence of pure- and mixed-gas CO_2 permeabilities of pristine TDA1-APAF [21] and TR 460 (1:1 CO_2/CH_4 mixture; 35 °C). Lines are drawn to guide the eye. Open points: pure-gas; closed points: mixed-gas.

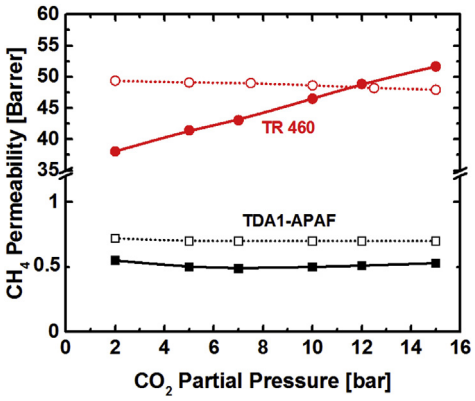

Fig. 9. Pressure-dependence of pure- and mixed-gas CH_4 permeabilities for pristine [21] and TR 460 (1:1 CO_2/CH_4 mixture, 35 °C). Lines are drawn to guide the eye. Open points: pure-gas; closed points: mixed-gas.

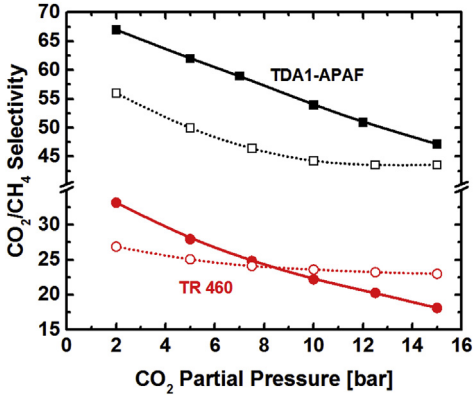

Fig. 10. Pressure-dependence of mixed-gas CO_2/CH_4 selectivities of pristine [21] and TR 460 samples (1:1 CO_2/CH_4 mixture, 35 °C). Lines are drawn to guide the eye: open points, pure-gas; closed points, mixed-gas.

4. Conclusions

In this work, a new TR membrane was prepared from a triptycene-based TDA1-APAF polyimide derived from 9,10-dimethyl-2,3,6,7-triptycene tetracarboxylic dianhydride (TDA1) and a commercial dihydroxyl-diamine (APAF) *via* one-step high-temperature solution imidization reaction. Pure-gas permeation data demonstrated that a TR membrane heated at 460 °C for 15 min (TR 460) showed significant increase in permeability due to large increases in diffusion coefficients for a variety of gases. A freshly tested TR 460 membrane showed excellent O_2 permeability of 311 Barrer coupled with O_2/N_2 selectivity of 5.4 and CO_2 permeability of 1328 Barrer with CO_2/CH_4 selectivity of 27. Physically aged TR 460 membrane samples tested over a period of 150 days showed a decrease in gas permeability (P_{O_2} = 185 Barrer) but with an increased O_2/N_2 selectivity of 6.3, which surpassed the 2008 upper bound and was close to the performance of other high-performance state-of-the-art PIM and PIM-PI membrane materials recently reported for the 2015 O_2/N_2 upper bound. Therefore, the PIM-PI-triptycene-based TR 460 membrane could find potential use in nitrogen production from air for a variety of demanding applications in the aircraft- and oil- and natural gas industries. The utilization of the TR membrane for CO_2 removal from natural gas is also commendable due to its high mixed-gas CO_2 permeability of ~1000 Barrer combined with CO_2/CH_4 selectivity of 22 at a typical CO_2 wellhead partial pressure of 10 bar.

Acknowledgments

The research reported in this publication was supported by funding from King Abdullah University of Science and Technology.

References

[1] P. Bernardo, E. Drioli, G. Golemme, Membrane gas separation: a review/state of the art, Ind. Eng. Chem. Res. 48 (2009) 4638–4663.
[2] R.W. Baker, K. Lokhandwala, Natural gas processing with membranes: an overview, Ind. Eng. Chem. Res. 47 (2008) 2109–2121.
[3] R.W. Baker, Future directions of membrane gas separation technology, Ind. Eng. Chem. Res. 41 (2002) 1393–1411.
[4] Y. Huang, D. Paul, Physical aging of thin glassy polymer films monitored by gas permeability, Polymer 45 (2004) 8377–8393.
[5] L.M. Robeson, Correlation of separation factor versus permeability for polymeric membranes, J. Membr. Sci. 62 (1991) 165–185.
[6] P.M. Budd, B.S. Ghanem, S. Makhseed, N.B. McKeown, K.J. Msayib, C.E. Tattershall, Polymers of intrinsic microporosity (PIMs): robust, solution-processable, organic nanoporous materials, Chem. Commun. (2004) 230–231.
[7] P.M. Budd, E.S. Elabas, B.S. Ghanem, S. Makhseed, N.B. McKeown, K.J. Msayib, C.E. Tattershall, D. Wang, Solution-processed, organophilic membrane derived from a polymer of intrinsic microporosity, Adv. Mater. 16 (2004) 456–459.
[8] P.M. Budd, K.J. Msayib, C.E. Tattershall, B.S. Ghanem, K.J. Reynolds, N.B. McKeown, D. Fritsch, Gas separation membranes from polymers of intrinsic microporosity, J. Membr. Sci. 251 (2005) 263–269.
[9] P.M. Budd, N.B. McKeown, D. Fritsch, Free volume and intrinsic microporosity in polymers, J. Mater. Chem. 15 (2005) 1977–1986.
[10] L.M. Robeson, The upper bound revisited, J. Membr. Sci. 320 (2008) 390–400.
[11] B.S. Ghanem, N.B. McKeown, P.M. Budd, J.D. Selbie, D. Fritsch, High-performance membranes from polyimides with intrinsic microporosity, Adv. Mater. 20 (2008) 2766–2771.
[12] B.S. Ghanem, N.B. McKeown, P.M. Budd, N.M. Al-Harbi, D. Fritsch, K. Heinrich, L. Starannikova, A. Tokarev, Y. Yampolskii, Synthesis, characterization, and gas permeation properties of a novel group of polymers with intrinsic microporosity: PIM-polyimides, Macromolecules 42 (2009) 7881–7888.
[13] J. Weber, O. Su, M. Antonietti, A. Thomas, Exploring polymers of intrinsic microporosity-microporous, soluble polyamide and polyimide, Macromol. Rapid Commun. 28 (2007) 1871–1876.
[14] X.H. Ma, R. Swaidan, Y. Belmabkhout, Y.H. Zhu, E. Litwiller, M. Jouiad, I. Pinnau, Y. Han, Synthesis and gas transport properties of hydroxyl-functionalized polyimides with intrinsic microporosity, Macromolecules 45 (2012) 3841–3849.
[15] Y. Rogan, L. Starannikova, V. Ryzhikh, Y. Yampolskii, P. Bernardo, F. Bazzarelli, J.C. Jansen, N.B. McKeown, Synthesis and gas permeation properties of novel spirobisindane-based polyimides of intrinsic microporosity, Polym. Chem. 4 (2013) 3813–3820.
[16] B.S. Ghanem, R. Swaidan, E. Litwiller, I. Pinnau, Ultra-microporous triptycene-based polyimide membranes for high-performance gas separation, Adv. Mater. 26 (2014) 3688–3692.
[17] N. Ritter, I. Senkovska, S. Kaskel, J. Weber, Intrinsically microporous poly(-imide)s: structure-porosity relationship studied by gas sorption and X-ray scattering, Macromolecules 44 (2011) 2025–2033.
[18] Y. Rogan, R. Malpass-Evans, M. Carta, M. Lee, J.C. Jansen, P. Bernardo, G. Clarizia, E. Tocci, K. Friess, M. Lanč, A highly permeable polyimide with enhanced selectivity for membrane gas separations, J. Mater. Chem. A 2 (2014) 4874–4877.
[19] X. Ma, O. Salinas, E. Litwiller, I. Pinnau, Novel spirobifluorene- and dibromospirobifluorene-based polyimides of intrinsic microporosity for gas separation applications, Macromolecules 46 (2013) 9618–9624.
[20] Y. Zhuang, J.G. Seong, Y.S. Do, H.J. Jo, Z. Cui, J. Lee, Y.M. Lee, M.D. Guiver, Intrinsically microporous soluble polyimides incorporating Tröger's base for membrane gas separation, Macromolecules 47 (2014) 3254–3262.
[21] F. Alghunaimi, B. Ghanem, N. Alaslai, M. Mukaddam, I. Pinnau, Triptycene dimethyl-bridgehead dianhydride-based intrinsically microporous hydroxyl-functionalized polyimide for natural gas upgrading, J. Membr. Sci. 520 (2016) 240–246.
[22] D.F. Sanders, Z.P. Smith, C.P. Ribeiro, R. Guo, J.E. McGrath, D.R. Paul, B.D. Freeman, Gas permeability, diffusivity, and free volume of thermally rearranged polymers based on 3, 3′-dihydroxy-4, 4′-diamino-biphenyl (HAB) and 2, 2′-bis-(3, 4-dicarboxyphenyl) hexafluoropropane dianhydride (6FDA), J. Membr. Sci. 409 (2012) 232–241.
[23] H.B. Park, C.H. Jung, Y.M. Lee, A.J. Hill, S.J. Pas, S.T. Mudie, E. Van Wagner, B.D. Freeman, D.J. Cookson, Polymers with cavities tuned for fast selective transport of small molecules and ions, Science 318 (2007) 254–258.
[24] H.B. Park, S.H. Han, C.H. Jung, Y.M. Lee, A.J. Hill, Thermally rearranged (TR) polymer membranes for CO_2 separation, J. Membr. Sci. 359 (2010) 11–24.
[25] Q. Liu, D.R. Paul, B.D. Freeman, Gas permeation and mechanical properties of thermally rearranged (TR) copolyimides, Polymer 82 (2016) 378–391.
[26] G.L. Tullos, J.M. Powers, S.J. Jeskey, L.J. Mathias, Thermal conversion of hydroxy-containing imides to benzoxazoles: polymer and model compound study, Macromolecules 32 (1999) 3598–3612.
[27] S.H. Han, N. Misdan, S. Kim, C.M. Doherty, A.J. Hill, Y.M. Lee, Thermally rearranged (TR) polybenzoxazole: effects of diverse imidization routes on physical properties and gas transport behaviors, Macromolecules 43 (2010) 7657–7667.
[28] M. Calle, C.M. Doherty, A.J. Hill, Y.M. Lee, Cross-linked thermally rearranged poly (benzoxazole-co-imide) membranes for gas separation, Macromolecules 46 (2013) 8179–8189.
[29] W. Liu, W. Xie, Acetate-functional thermally rearranged polyimides based on 2, 2-bis (3-amino-4-hydroxyphenyl) hexafluoropropane and various dianhydrides for gas separations, Ind. Eng. Chem. Res. 53 (2013) 871–879.
[30] S. Kim, Y.M. Lee, Rigid and microporous polymers for gas separation membranes, Prog. Polym. Sci. 43 (2015) 1–32.
[31] C.H. Jung, J.E. Lee, S.H. Han, H.B. Park, Y.M. Lee, Highly permeable and selective poly (benzoxazole-co-imide) membranes for gas separation, J. Membr. Sci. 350 (2010) 301–309.
[32] S. Luo, J. Liu, H. Lin, B.A. Kazanowska, M.D. Hunckler, R.K. Roeder, R. Guo, Preparation and gas transport properties of triptycene-containing polybenzoxazole (PBO)-based polymers derived from thermal rearrangement (TR) and thermal cyclodehydration (TC) processes, J. Mater. Chem. A 4 (2016) 17050–17062.
[33] S. Li, H.J. Jo, S.H. Han, C.H. Park, S. Kim, P.M. Budd, Y.M. Lee, Mechanically robust thermally rearranged (TR) polymer membranes with spirobisindane for gas separation, J. Membr. Sci. 434 (2013) 137–147.
[34] R. Swaidan, X. Ma, E. Litwiller, I. Pinnau, High pressure pure-and mixed-gas separation of CO_2/CH_4 by thermally-rearranged and carbon molecular sieve membranes derived from a polyimide of intrinsic microporosity, J. Membr. Sci. 447 (2013) 387–394.
[35] H. Shamsipur, B.A. Dawood, P.M. Budd, P. Bernardo, G. Clarizia, J.C. Jansen, Thermally rearrangeable PIM-polyimides for gas separation membranes, Macromolecules 47 (2014) 5595–5606.
[36] X. Ma, O. Salinas, E. Litwiller, I. Pinnau, Pristine and thermally-rearranged gas separation membranes from novel o-hydroxyl-functionalized spirobifluorene-based polyimides, Polym. Chem. 5 (2014) 6914–6922.
[37] B. Ghanem, F. Alghunaimi, X. Ma, N. Alaslai, I. Pinnau, Synthesis and characterization of novel triptycene dianhydrides and polyimides of intrinsic microporosity based on 3, 3′-dimethylnaphthidine, Polymer 101 (2016) 225–232.
[38] D.F. Sanders, R. Guo, Z.P. Smith, Q. Liu, K.A. Stevens, J.E. McGrath, D.R. Paul, B.D. Freeman, Influence of polyimide precursor synthesis route and ortho-position functional group on thermally rearranged (TR) polymer properties: conversion and free volume, Polymer 55 (2014) 1636–1647.
[39] K. O'Brien, W. Koros, T. Barbari, E. Sanders, A new technique for the measurement of multicomponent gas transport through polymeric films, J. Membr. Sci. 29 (1986) 229–238.
[40] X. Ma, R. Swaidan, B. Teng, H. Tan, O. Salinas, E. Litwiller, Y. Han, I. Pinnau, Carbon molecular sieve gas separation membranes based on an intrinsically microporous polyimide precursor, Carbon 62 (2013) 88–96.
[41] R. Guo, D.F. Sanders, Z.P. Smith, B.D. Freeman, D.R. Paul, J.E. McGrath, Synthesis and characterization of thermally rearranged (TR) polymers: effect of glass transition temperature of aromatic poly (hydroxyimide) precursors on TR process and gas permeation properties, J. Mater. Chem. A 1 (2013) 6063–6072.
[42] M. Calle, A.E. Lozano, Y.M. Lee, Formation of thermally rearranged (TR) polybenzoxazoles: effect of synthesis routes and polymer form, Eur. Polym. J. 48 (2012) 1313–1322.
[43] K.D. Dorkenoo, P.H. Pfromm, Accelerated physical aging of thin poly[1-(trimethylsilyl)-1-propyne] films, Macromolecules 33 (2000) 3747–3751.
[44] P.H. Pfromm, The impact of physical aging of amorphous glassy polymers on gas separation membranes, in: Y. Yampolskii, I. Pinnau, B.D. Freeman (Eds.), Materials Science of Membranes for Gas and Vapor Separation, John Wiley & Sons, 2006, pp. 293–306.
[45] R. Swaidan, B. Ghanem, I. Pinnau, Fine-tuned intrinsically ultramicroporous polymers redefine the permeability/selectivity upper bounds of membrane-based air and hydrogen separations, ACS Macro Lett. 4 (2015) 947–951.
[46] R. Swaidan, B. Ghanem, E. Litwiller, I. Pinnau, Effects of hydroxyl-functionalization and sub-Tg thermal annealing on high pressure pure-and mixed-gas CO_2/CH_4 separation by polyimide membranes based on 6FDA and triptycene-containing dianhydrides, J. Membr. Sci. 475 (2015) 571–581.
[47] R. Swaidan, B. Ghanem, M. Al-Saeedi, E. Litwiller, I. Pinnau, Role of intrachain rigidity in the plasticization of intrinsically microporous triptycene-based polyimide membranes in mixed-gas CO_2/CH_4 separations, Macromolecules 47 (2014) 7453–7462.
[48] F. Alghunaimi, B. Ghanem, N. Alaslai, R. Swaidan, E. Litwiller, I. Pinnau, Gas permeation and physical aging properties of iptycene diamine-based microporous polyimides, J. Membr. Sci. 490 (2015) 321–327.
[49] N. Alaslai, B. Ghanem, F. Alghunaimi, E. Litwiller, I. Pinnau, Pure-and mixed-gas permeation properties of highly selective and plasticization resistant hydroxyl-diamine-based 6FDA polyimides for CO_2/CH_4 separation, J. Membr. Sci. 505 (2016) 100–107.
[50] N. Du, H.B. Park, G.P. Robertson, M.M. Dal-Cin, T. Visser, L. Scoles, M.D. Guiver, Polymer nanosieve membranes for CO_2-capture applications, Nat. Mater. 10 (2011) 372–375.
[51] K.L. Gleason, Z.P. Smith, Q. Liu, D.R. Paul, B.D. Freeman, Pure-and mixed-gas permeation of CO_2 and CH_4 in thermally rearranged polymers based on 3, 3′-dihydroxy-4, 4′-diamino-biphenyl (HAB) and 2, 2′-bis-(3, 4-dicarboxyphenyl) hexafluoropropane dianhydride (6FDA), J. Membr. Sci. 475 (2015) 204–214.